APPLIED AND ENVIRONMENTAL MICROBIOLOGY, Feb. 2004, p. 771–780 Vol. 70, No. 2
0099-2240/04/$08.00+0 DOI: 10.1128/AEM.70.2.771–780.2004

Determination of Cu Environments in the Cyanobacterium *Anabaena flos-aquae* by X-Ray Absorption Spectroscopy

X. C. Kretschmer,[1]* G. Meitzner,[2] J. L. Gardea-Torresdey,[1] and R. Webb[1]

Department of Environmental Science and Engineering[1] and Materials Research and Technology Institute,[2] The University of Texas at El Paso, El Paso, Texas 79968

Received 18 July 2003/Accepted 4 November 2003

Whole cells and peptidoglycan isolated from cell walls of the cyanobacterium *Anabaena flos-aquae* were lyophilized and used at pH 2 and pH 5 in Cu(II) binding studies. X-ray absorption spectra measured at the Cu K-edge were used to determine the oxidation states and chemical environments of Cu species in the whole-cell and peptidoglycan samples. In the whole-cell samples, most of the Cu retained at both pH values was coordinated by phosphate ligands. The whole-cell fractions contained significant concentrations of Cu(I) as well as Cu(II). An X-ray absorption near-edge spectrum analysis suggested that Cu(I) was coordinated by amine and thiol ligands. An analysis of the peptidoglycan fractions found that more Cu was adsorbed by the peptidoglycan fraction prepared at pH 5, due to increased chelation by amine and carboxyl ligands. The peptidoglycan fractions, also referred to as the cell wall fractions, contained little or no Cu(I). The Cu loading level was 30 times higher in the cell wall sample prepared at pH 5 than in the sample prepared at pH 2. Amine and bidentate carboxyl ligands had similar relative levels of importance in cell wall peptidoglycan samples prepared at both pH values, but phosphate coordination was insignificant.

Heavy metals damage the environment since they are nonbiodegradable and have toxic effects on plants, animals, and humans. Precipitation, coagulation, membrane-based processes, and ion exchange are some of the current approaches to the remediation of contaminated sites, but these methods are expensive and lose effectiveness as metal concentrations fall (54). The use of microbes for the bioremediation of trace metals has shown potential for enabling a site to meet regulatory specifications. Experiments have demonstrated the ability of bacteria to immobilize and concentrate metal ions (6, 14, 28, 37, 46).

Mechanisms by which cells accumulate, sequester, and detoxify metals have been investigated. One indirect approach has been the determination of uptake and retention as a function of pH or competition with some other cation (14, 16, 20, 35). Another has been to chemically modify plant or cell matter (for example, by esterification) to render specific classes of prospective ligands unavailable and to evaluate the impact on metal binding capacity (7, 21). In a study of binding sites in cell walls of gram-positive bacteria, teichoic acid, presenting phosphate sites, was extracted with aqueous alkali in order to quantify its contribution to metal binding (7).

The chemical studies described are informative but involve many assumptions due to the complexity of biological systems. Also, because of that complexity, few analytical probes can illuminate the chemistry of metals associated with cells. X-ray absorption spectroscopy (XAS) is element specific, returning information for a single atomic number in an arbitrarily complicated mixture (52). XAS is nondestructive, and no sample reduction or digestion is required which would alter the chemistry of the element of interest. XAS can be used to determine the oxidation state or states of the element as well as the physical structure of sites surrounding it to a radius of about 5 Å. Much research has been accomplished recently in the study of cyanobacterial protein interactions with metals, metal availability in cyanobacteria, and Cu homeostasis in other microorganisms (12, 62, 69). We are concerned here with metals adsorbed by lyophilized cells and not essential metals that are present, for example, as metalloenzyme cofactors in live cells (15, 17).

Several groups have used XAS to investigate the chemistry of accumulated metals in biological samples. Previous XAS studies of Cu in plants have examined *Solanum elaeagnifolium* (silverleaf nightshade) (68), hops (systematic name not given) (49), and *Larrea tridentata* (creosote bush) (22, 51). These reports identified only the immediate oxygen, nitrogen, or sulfur neighboring atoms and inferred hydroxyl, amine, carboxyl, or thiol ligands. Conclusions were corroborated by investigations of the effect of esterifying prospective ligands upon Cu binding. Decreased Cu binding was interpreted as evidence that a carboxyl was the principal ligand. However, it is not clear that the esterification chemistry was specific for carboxyl groups. An extended X-ray absorption fine structure (EXAFS) study of Zn coordination in anaerobic bacteria concluded that XAS is capable of discriminating thiol, O/N, and phosphate ligands (72), but did not quantify the respective fractions coordinating Zn in the samples. A study by Sarret et al. (60) of Zn(II) and Pb(II) binding by cell walls from the fungus *Penicillium chrysogenum* combined titration with the metal cations of binding sites and EXAFS of adsorbed cations. Carboxyl-Pb complexes were formed at low Pb concentrations, followed by $(PO_4)_n$-Pb complexes. In contrast, Zn saturated PO_4^{3-} sites first. The study developed a detailed model for metal binding sites. Nevertheless, most XAS studies of cell-bound Cu and other metals have presented a simplified picture, approximating the metal environment by the presumably most abundant ligand and assuming the extended structure of this ligand. In this report, we describe the use of a more elaborate model to interpret the EXAFS of Cu bound by purified peptidoglycan of cell walls and to differentiate and quantify amine and carboxyl

* Corresponding author. Mailing address: Department of Biological Sciences, The University of Texas at El Paso, El Paso, TX 79968. Phone: (915) 747-6876. Fax: (915) 747-5808. E-mail: xkretschmer@utep.edu.

ligands. In addition, some structural information was obtained that describes the ligands.

MATERIALS AND METHODS

Whole-cell isolation. *Anabaena flos-aquae* (ATCC 22664) was cultured in liquid BG-11 medium (2) and grown autotrophically as previously described (37). Cells were collected by using a continuous-flow Sorvall centrifuge, washed with sterile distilled water, and lyophilized in a Labconco freeze-dryer prior to reaction for 1 h with a 1,000-ppm Cu(II) ion solution from $CuSO_4$. After the adsorption of Cu, samples were washed three times with deionized water and again lyophilized.

Cell wall peptidoglycan isolation. *A. flos-aquae* (ATCC 22664) was cultured in liquid BG-11 medium and grown autotrophically as previously described (37). Cell walls were isolated by ultracentrifugation according to previously described procedures (37). Though they are referred to here as cell wall samples, the samples comprised only the purified peptidoglycan fraction of cell walls and did not include the outer membrane fraction of cell envelopes. Samples of 100 mg of lyophilized *Anabaena* sp. peptidoglycan were washed twice with 0.01 M hydrochloric acid, followed by two washes with deionized water, which served to strip any adventitiously bound metal ions. Samples were then resuspended in 30 ml of 1,000-ppm Cu(II) metal ion (from $CuSO_4 \cdot 5H_2O$) solution at pH 5 or pH 2. Binding was allowed to occur for 1 h, with gentle agitation. With three washes in deionized water, samples were prepared for flame atomic absorption analysis and XAS analysis as previously described (37).

XAS measurements. Cu K-edge X-ray absorption spectra were measured on wiggler beamline 7-3 (1.8-T wiggler field) at the Stanford Synchrotron Radiation Laboratory (SSRL). The storage ring SPEAR was operated at 3 GeV with a current of 50 to 100 mA. The double-crystal monochromator used Si (220) crystals and was detuned to decrease the output intensity by 50% to reject harmonics. The resolution was set at about 1 eV by 2-mm vertical and 20-mm horizontal apertures in front of the monochromator. The beamline was controlled by the data collection program XAS_COLLECT. The intensity of X-rays incident on the sample was monitored with an N_2-filled ion chamber. For energy calibration, an N_2-filled ion chamber positioned beyond the sample (I_1) monitored transmission and a second N_2-filled ion chamber (I_2) measured a calibration spectrum from a 7.5-μm Cu foil. The sample fluorescence intensity was measured with a Canberra 13-element Ge detector, and all 13 channels (I_F) were averaged in the analyzed spectra. The sample spectra were analyzed with the term $(\Sigma I_F)/I_o$ and the calibration spectrum was analyzed with the term $\ln(I_1/I_2)$. All samples were loaded into 0.5-mm-diameter Al sample cells, sealed with Kapton tape, and frozen by immersion in liquid N_2. During data collection, samples were kept at 10 K in an Oxford Instruments liquid He flow cryostat and oriented at 45° to the X-ray beam to improve the fluorescence signal. Spectra were measured starting at 8,730 eV, with a 10-eV increment and 1-s integration time per point to 8,940 eV; a 0.35-eV increment and 1-s integration time from 8,940 to 9,010 eV; and a 0.05 $Å^{-1}$ increment from 2.8 to 13 $Å^{-1}$ [$K/Å^{-1} \cong 0.5 (E - E_o)^{1/2}$; E_o = 8,979 eV]. The integration time in the EXAFS region from 2.8 to 13 $Å^{-1}$ was scaled from 1 to 5 s per point according to a K^2 weighting scheme.

Cu concentrations. Cu loading levels in pH 5 whole-cell and cell wall samples were determined by atomic absorption analysis as reported previously (37). Cu concentrations in all the samples and resins were inferred from the changes in absorbance (ΔA) across the Cu K-edges. The step heights, shown in Table 1, were the differences between the absorbance values in the pre-edge and postedge polynomial fits, extrapolated through and calculated at the E_o values for each spectrum, also shown in Table 1. The step heights are directly proportional to absolute Cu concentrations since all of the samples were prepared for spectroscopy in the same way, presented equal path lengths ($x \cong 0.7$ mm), and had low total absorbance values. The absolute concentrations (c) of Cu in the samples were obtained from step heights by application of the Beer-Lambert Law: $\Delta A = \Delta\mu \times x \times c$, where $\Delta\mu$ is the intrinsic change in absorbance across a Cu K-edge (251 $cm^2\ g^{-1}$) (45). Aside from the convenience that the information was obtained in conjunction with the measurement of the X-ray absorption spectra, this analysis had the advantages that it was nondestructive, required no special sample preparation that could affect the accuracy of the result, and had no interference.

Procedures for analysis of XANES. The analyzed spectra represent a single sweep or the average of up to three sweeps and the averages of the 13 channels measured by the Ge detector. The energy scales were calibrated by defining the first inflection point in the Cu foil spectrum as 8,979 eV. Edge energies for the sample spectra, reported in Table 1, were also defined at the first inflection points. The X-ray absorption near-edge spectra (XANES) were extracted by subtracting a linear regression to the pre-edge region, from 8,865 to 8,960 eV, from the entire spectra. The spectra were then normalized by a fifth-order polynomial fitted to the postedge region, from 9,030 to 9,650 eV. The analysis of XANES used the range from 8,900 to 9,100 eV.

TABLE 1. Cu K-edge positions, identified by the first inflection points, for Cu standard compounds and Cu samples[a]

Sample	Cu K-edge energy (eV)	Cu K-edge step height (ΔA)
Cu foil	8,979	
Cu_2O	8,980	
$Cu(CH_3COO)_2 \cdot H_2O$	8,990	
$CuSO_4 \cdot 5H_2O$	8,988	
Thiol resin, pH 5	8,981	
Amine resin, pH 2	8,981	0.027
Amine resin, pH 5	8,985	0.82
Carboxyl resin, pH 2	8,987	0.0075
Carboxyl resin, pH 5	8,991	0.049
Whole cell, pH 2	8,982	0.91
Whole cell, pH 5	8,982	2.3
Cell wall, pH 2	8,986	0.29
Cell wall, pH 5	8,986	3.5

[a] Binding energies, corresponding to edge energies, increase as core electrons are deshielded by oxidation. Cu step heights are proportional to Cu concentrations in the samples.

Reference spectra were measured from standard compounds Cu metal (7.5-μm-long foil), Cu_2O, $Cu(CH_3COO)_2 \cdot H_2O$ (99.7%) (Sigma Chemicals), $CuSO_4 \cdot 5H_2O$ (98 to 102%) (Spectrum Chemicals), and $CuHPO_4$. $CuHPO_4$ was the gelatinous blue precipitate formed at the diffusional interface between 0.1 M aqueous $H(NH_4)_2PO_4$ (pH ≅ 5) and 0.1 M aqueous $Cu(OAc)_2 \cdot H_2O$ and digested in the mother liquor at 375 K in air. We do not have an X-ray diffraction determination of the phase since the amount collected was small, but we suspect it was amorphous. Other reference spectra were measured from Cu-exchanged carboxyl (Diaion WT01S), amine (Diaion CR20), and thiol-type (Doulite GT73) chelating resins. All resins used in this study were obtained from Supelco (Bellefonte, Pa.). The XANES from each standard compound and resin were tested against the sample spectra by principal component analysis (PCA) (44, 56). Successful reconstruction of a reference spectrum using the components calculated from the sample spectra by the PCA algorithm suggests that species resembling the standard compounds are represented among the species contributing to the sample spectra. Fractions of Cu(I) and Cu(II) oxidation states were determined by linear combination fits of sample spectra, using reference spectra selected by successful PCA target-transform reconstruction. The spectrum from a sample that is a mixture is the sum of the spectra from the components, weighted by their respective atomic fractions (47).

Procedures for analysis of EXAFS. All spectrum analyses were performed by use of the program WinXAS, version 2.1 (57, 58). The Fourier transform (FT) magnitude plots were prepared according to the following procedure. After the energy scale was calibrated by defining the first inflection point in the calibration spectrum as 8,979 eV, a linear fit to the pre-edge region, from 8,810 to 8,940 eV, was subtracted from the entire spectrum. The spectrum was normalized by a fifth-order polynomial fit to the postedge region, from 9,160 to 9,640 eV. The EXAFS region was converted to units of $Å^{-1}$ by using the edge energy values in Table 1 and was weighted by K^3, and a cubic spline polynomial with four knots fitted to the range from 1.3 to 13.1 $Å^{-1}$ was subtracted. The residual EXAFS was weighted by K^1, a Hanning window was applied to the first and last 10% of the range, and the data were Fourier transformed from 1.5 to 12.5 $Å^{-1}$.

Two approaches were taken for fitting the EXAFS to obtain structural information. Some EXAFS spectra were fitted in real space by using experimental phase shift and back scattering amplitude functions derived from other spectra. In other cases, the input was created by FEFF, version 8.1 (3, 4; FEFF Project, University of Washington, Seattle, Wash.), to describe a noncrystalline structural model, e.g., a phosphate or bidentate carboxylate ligand. Then the single-scattering paths calculated by FEFF were refined in real space, from 0 to 8 Å, against the experimental EXAFS. Structural parameters describing ligands were correlated to retain the essential features of the ligands and to limit the numbers of free variables, but to allow the ligand number to increase or decrease and to allow ligand translation with respect to the metal center.

RESULTS

Cu concentrations. The Cu loading in the whole-cell sample prepared in pH 5 aqueous 1,000-ppm Cu^{2+} was 26.8 mg g^{-1}, as

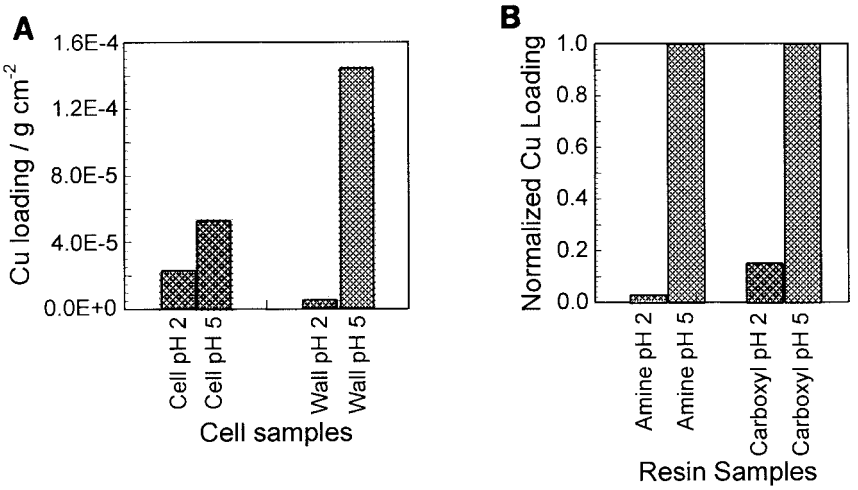

FIG. 1. Cu K-edge step heights showed that the whole cells and cell wall peptidoglycan groups both retained less Cu at low pH (A), as did the amine and carboxyl resins used as standards (B). The cell wall peptidoglycan sample and resin standards showed a similar dependence of Cu adsorption on the pH of the solution.

determined by atomic absorption analysis and as previously reported (37). The Cu concentrations in all the samples and resins were inferred from the changes in absorbance (ΔA) across the Cu K-edges, as described in the appendix.

Figure 1 compares Cu loading levels in whole-cell samples prepared at pH 2 and pH 5. The relative concentrations of Cu on an amine chelation resin, adsorbed at pH 2 and pH 5, are shown for comparison. The whole-cell sample retained 2.5 times as much Cu at pH 5 as at pH 2, thus illustrating relatively weak pH dependence. We infer that this pH-independent site was present to a maximum of about 8% in the cell wall fraction. In contrast, the purified cell wall peptidoglycan fraction was similar to the amine resin, retaining 13 times as uch Cu at pH 5 as at pH 2.

Based on the close similarity of the EXAFS from the pH 2 and pH 5 cell wall samples (37), we believe that all the sites at both pH values were of the same types in the cell wall fraction.

Insight into the nature of the pH-sensitive sites is gained from the pH dependence of the Cu loading levels on amine- and carboxyl-type resins. The figure indicates that the amine resin retained about 30 times more Cu at pH 5 than at pH 2. The carboxyl resin retained about seven times more Cu at pH 5 than at pH 2. At both pH values, the amine resin retained substantially more Cu than the carboxyl resin, but this has been normalized out of the graph since it may reflect site densities on the resins rather than intrinsic strengths of binding.

Cu XANES. In order to gain more insight into the nature of the pH-dependent binding sites, Cu XANES was performed. The Cu K-edge positions in Table 1, reflecting higher binding energies for 1s electrons on more oxidized Cu (38), establish that both Cu(II) and Cu(I) occurred among the whole-cell samples and the resins. Of course, the edge position is a single parameter to describe samples that may contain Cu in multiple oxidation states, and the results in Table 1 reflect the lowest Cu oxidation state (which would have the lowest edge energy) present at a substantial concentration. Cu(II) dominated in the cell wall samples.

The XANES region of an X-ray absorption spectrum is a fingerprint of the chemical species of the absorbing atoms. We used the target transform application of PCA to assess the similarity between Cu species in the whole-cell and cell wall peptidoglycan samples, the amine, carboxyl, and thiol resins, and several reference compounds (44, 56). The successful reconstruction of a reference spectrum using the components calculated from the sample spectra by the PCA algorithm suggests that species resembling the standard compounds are represented among the species contributing to the sample spectra. The PCA reconstructions of XANES spectra from Cu(I) and Cu(II) standards are shown in Fig. 2. The PCA reconstructions of XANES spectra from Cu(II) standards were extremely accurate for the XANES of Cu in the amine and carboxyl resins prepared at pH 5 and were less successful for XANES from the $CuSO_4 \cdot 5H_2O$, $Cu(OAc)_2 \cdot H_2O$, and $CuHPO_4$ standard Cu(II) compounds. The Cu sites in the samples are not believed to exactly match those in any of the reference compounds, but the success of the reconstructions reflects that Cu in all of them occupies complex oxygen coordinated environments. In anhydrous $Cu_3(PO_4)_2$, the two Cu sites are distorted trigonal bipyramidal and distorted square planar sites (61). In $Cu(OAc)_2 \cdot H_2O$, the Cu site is a distorted square pyramid (70). In $CuSO_4 \cdot 5H_2O$, the two Cu sites are both distorted octahedra, between them presenting six Cu-O distances between 1.95 and 2.40 Å (5). All of these compounds possess Cu(II) in sites with several Cu-O distances in a narrow range, and the corresponding XANES is a complex average for each case.

The reconstructions of Cu(I) standards show that in the case of Cu_2O and CuCl, the edge positions were correctly reproduced. The Cu(I) edge position and pre-edge peak were correctly reconstructed by the PCA target transformation. In general, the XANES of the compounds was not very well reconstructed by components from the XANES of whole cells.

Although supplied in the form of Cu(II) from aqueous $CuSO_4$, the Cu retained by the pH 2 amine resin and pH 5 thiol resin was mainly Cu(I). As shown in Fig. 2, the main features of both of these spectra were reconstructed from components generated by PCA of the whole-cell spectra. We conclude that the Cu(I) in the whole-cell samples was in an amine or thiol coordination environment, or possibly both.

Finally, the PCA target transform failed to reconstruct the

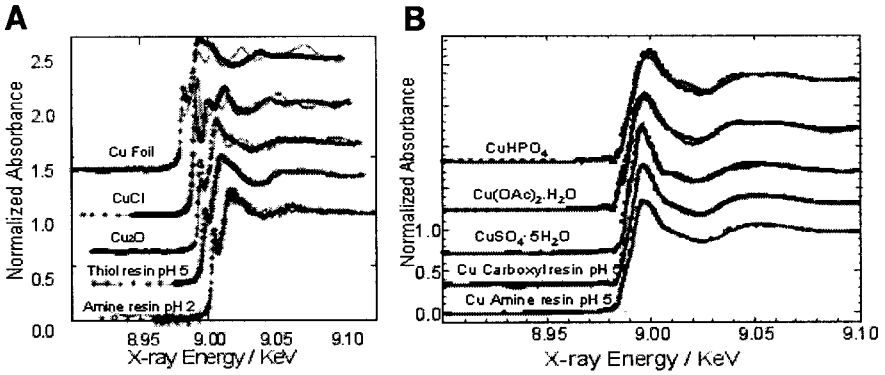

FIG. 2. (A) Target transform reconstructions (dots) of Cu metal and Cu(I) reference spectra from components generated by PCA of whole-cell and cell wall peptidoglycan sample XANES. (B) Target transform reconstructions (dots) of Cu(II) and Cu metal reference spectra from components generated by PCA of whole-cell and cell wall peptidoglycan sample XANES. Only the resin reconstructions indicate sites of the same structure.

XANES of Cu metal. On that basis, we reject the presence of Cu(0) as Cu nanoparticles in any of the samples.

The fractions of Cu(I) in the whole-cell samples were determined by linear combination fits, using the XANES from the amine resins prepared at pH 2 and pH 5 as reference spectra. As shown in Table 2, the cell sample at pH 5 contained as much as half Cu(I). The values for fractions of Cu(I) in Table 2 could be too high by an indeterminate amount. This is because we cannot eliminate the possibility that our standard for Cu(I), the pH 2 amine resin, also contained Cu(II). In that case, the fraction of Cu(II) in the standard will be reported as Cu(I) in the whole-cell samples. However, an inspection of the pH 2 amine resin XANES spectrum indicated that the contribution from Cu(II) must be small.

Cu EXAFS. Fig. 3 compares the EXAFS spectra of experimental whole-cell and cell wall samples at pH 2 and pH 5 to those of the amine and carboxyl resins at pH 5. Analysis of Cu K-edge XANES gave an incomplete picture of Cu environments in the whole-cell and cell wall peptidoglycan samples, showing mainly that Cu(II) sites did not match those in materials for which we had X-ray crystal structures. Consequently, we refined structural models based on amine, carboxyl, and phosphate coordination against the Cu EXAFS.

The comparison of FT magnitudes from standard compounds with sample EXAFS FTs in Fig. 4 indicates that the coordination of Cu in the samples did not match the Cu coordination in the standard compounds, which were crystalline bulk chemicals. This is not surprising; in $Cu(OAc)_2 \cdot H_2O$, for example, pairs of Cu cations are bridged by four acetate ligands and capped by waters of hydration, giving each Cu a square pyramidal coordination by monodentate carboxylates. That is not necessarily the expected configuration in the cell environment, in which carboxyl ligands are tethered and Cu is much more dilute. The extremely precise PCA reconstructions of the XANES from the Cu on amine and carboxyl resins shown in Fig. 2, together with the strong pH sensitivity of the Cu loadings and the presence in cells of those types of ligands, identified those resin samples as appropriate Cu(II) standards for the analysis of EXAFS. We modeled amine and carboxyl coordination by fitting the cell wall peptidoglycan EXAFS with phase shift functions and back-scattering amplitude functions extracted from the frequency range of 0- to 4-Å components of the EXAFS of the amine and carboxyl resins. The determinations of phase shift and back-scattering amplitude functions used nominal coordination numbers and interatomic distances of 4 and 2 Å, respectively. The fits then varied the coordination numbers, interatomic distances, and edge energies to determine the distribution of coordination between the amine and carboxyl ligands. The EXAFS from the resins were finally fit

TABLE 2. Distributions between Cu(I) and Cu(II) oxidation states, reported here as percentages with standard deviations, determined by linear combination fits to XANES spectra from the samples[a]

Sample	Amt of Cu(I)	Amt of Cu(II)
Whole cell, pH 2	28 ± 0.3	73 ± 0.2
Whole cell, pH 5	45 ± 0.3	55 ± 0.2
Cell wall peptidoglycan, pH 2	13 ± 0.4	87 ± 0.1
Cell wall peptidoglycan, pH 5	7 ± 0.2	93 ± 0.2

[a] The standard spectrum for Cu(I) was from Cu on the pH 2 amine resin, and the one for Cu(II) was from Cu on the pH 5 amine resin. The fractions of Cu(I) may be too high since our Cu(I) standard may have contained Cu(II). The value of 13% Cu(I) in the pH 2 cell wall sample is within the level of uncertainty in the determinations and is considered not significant.

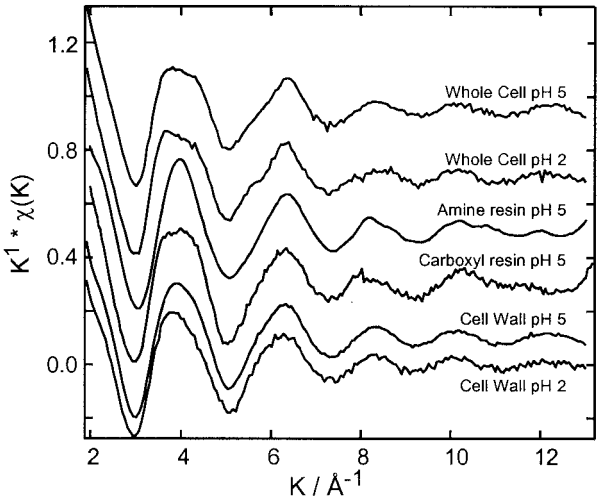

FIG. 3. K^1-weighted EXAFS data as a function of k-space of cell wall peptidoglycan samples at pH 2 and pH 5, whole cells at pH 2 and pH 5, and amine and carboxyl resins at pH 5.

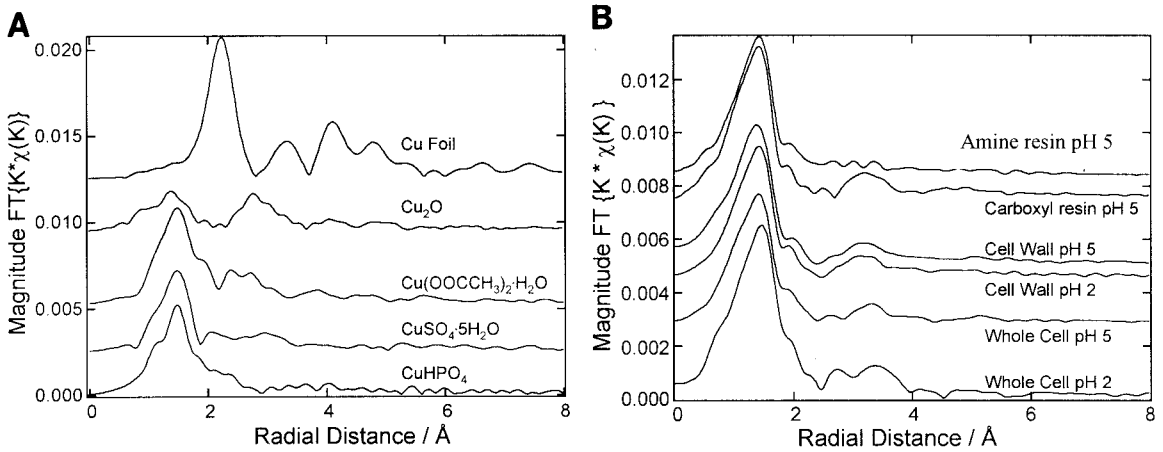

FIG. 4. Magnitudes of K^1-weighted Fourier-transformed Cu K-edge EXAFS from several reference compounds (A) and cell wall peptidoglycan, whole cells, and resin samples (B) also used as reference materials. Cu environments in cell wall samples at two different pH values were near identical. Structural differences among whole-cell samples at two different pH values and amine- and carboxyl-type resins are evident.

with FEFF-simulated amine or carboxyl models to determine the structures in the resins. This approach was similar to fitting the cell wall EXAFS with linear combinations of resins EXAFS, but accommodated contraction or expansion of the coordination sphere by the distance variable (actually found to be <5%). The combined use of experimental and FEFF information to fit the peptidoglycan EXAFS means that the structural information we report here is based on EXAFS from three samples rather than from a single sample. The implicit assumption, which is supported by the success of XANES and EXAFS fits, is that Cu binding sites in the amine and carboxyl resins closely resembled most of the sites in the cell wall samples.

We also required a model for phosphate coordination since it has been suggested in the literature (18) as a reservoir for accumulated metals in whole cells. This type of environment is postulated as the pH-insensitive site, since Cu phosphates are not dissociated at pH 2 to pH 5 (71). As the starting point for this model, we simulated the EXAFS of a Cu atom with one PO_4^{3-} ligand in the configuration presented by the square planar site in anhydrous $Cu_3(PO_4)_2$ (61). A phosphate group, defined by one path to the phosphorus core and four paths to the four oxygens, was refined against the sample EXAFS. The coordination numbers describing the four oxygens and one phosphorus were held to the same values to allow our phosphate ligand to multiply but to prevent it from degenerating into some P_xO_y species for which y/x does not equal four. Four Cu-O distances and one Cu-P distance were allowed to vary to enable the phosphate to rotate with respect to the Cu.

Fits with carboxyl-plus-amine ligands captured the major features in the cell wall EXAFS below 4 Å (Fig. 5A). A discrepancy at 3.5 Å suggested that there are structural motives that are not described by the amine and carboxyl resins, but on the whole the fits were good. As shown in Table 3, the fits found similar amounts of amine and carboxyl coordination in the cell wall samples. The amine and carboxyl resins used as standards contained Cu in exclusively amine and carboxyl binding sites, respectively. However, the success of the fits does not imply that Cu in the cell wall peptidoglycan samples was co-

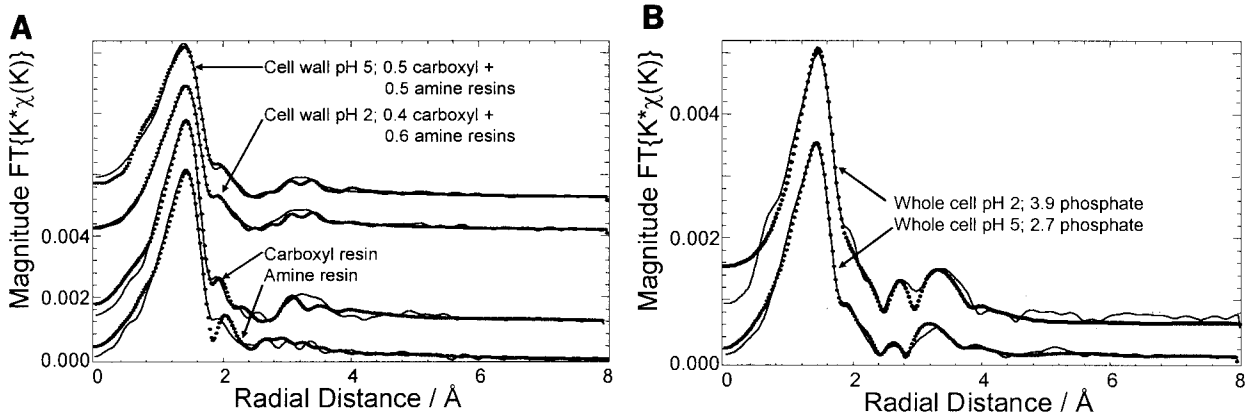

FIG. 5. (A) Top two traces show fits (dots) to EXAFS from the cell wall peptidoglycan samples using phase shift and back-scattering amplitude functions derived from the EXAFS of Cu on the carboxyl and amine resins. Fits to weak features beyond the first peak are significant since the corresponding paths were not independently refined. The bottom two traces show the fits (dots) to the Cu EXAFS from amine and carboxyl resins, finding four secondary amine ligands with ethylene bridges and two bidentate carboxyl ligands, respectively. (B) Fits (dots) to the whole-cell EXAFS used FEFF-generated inputs based on a model comprising a monodentate phosphate anion.

TABLE 3. Distribution between amine and carboxyl groups with standard deviations, of the coordination environments of Cu in the cell wall peptidoglycan samples[a]

Sample	% Amine resin, pH 5	% Carboxyl resin, pH 5
Cell wall, pH 2	0.6 ± 0.01	0.4 ± 0.01
Cell wall, pH 5	0.5 ± 0.2	0.5 ± 0.2

[a] The cell wall peptidoglycan EXAFS was fit using phase shift and backscattering amplitude functions derived from the pH 5 amine and carboxyl resins. The coordination numbers returned by the fits were normalized to express the results as fractions of the two different Cu environments.

ordinated by either exclusively amine or exclusively carboxyl ligands. The result is also consistent with any distribution of mixed coordination.

The magnitudes of real space fits to Cu EXAFS FTs from whole-cell samples are also shown in Fig. 5B. Our initial model comprised simulations of phosphate plus amine and carboxyl ligands, but it was unmanageably complicated and probably overly demanding of the limited information content of the EXAFS. In any case, the amine and carboxyl models originally presented along with the phosphate were rejected in favor of phosphate coordination. Consequently, the fits shown in Fig. 5B reflect only phosphate coordination. In the case of the pH 2 sample, in which amine and carboxyl coordination are expected to be at a minimum, the model finds an average of four phosphate ligands per Cu cation (see appendix). At pH 5, this value is only 2.7. The apparent decrease in the phosphate coordination is consistent with the increased coordination of Cu by carboxyl and amine groups and reflects the inability of the phosphate model to describe those types of ligands. This model cannot identify site symmetry.

To further understand the meaning of the fits to the cell wall samples with EXAFS from the amine and carboxyl resins, we fit the resin EXAFS by refining FEFF simulations of four amine ligands with pendant ethyl residues or bidentate acetate ligands. Coordination by monodentate as well as bidentate carboxyls may be present. However, fitting with a model that included both modes established that a bidentate carboxyl dominated. In both the amine and carboxyl fits, the simplest model comprising four oxygen or nitrogen atom neighbors found convincingly good fits, with first-shell coordination numbers around 2.5. This seemed unlikely for Cu(II). To understand the result, we fit the Cu EXAFS from Cu phthalcyanine, which holds Cu in rigid square planar coordination by nitrogen ligands. Interference among signals from the nearest nitrogen atoms and proximate alkyl skeleton had to be described in order to correctly simulate the EXAFS and find the true Cu-N coordination number of four. For this reason, we included more than one shell beyond the atoms immediately coordinating the Cu in the amine and carboxyl fits. The fits, shown as the two bottom traces in Fig. 5A and described in the appendix, capture the main features in the FT magnitude plots out to about 4 Å. Molecular models that incorporate the coordination numbers and interatomic distances found by the fits are shown in Fig. 6A. Figure 6B shows a molecular model that incorporates the bond length and coordination information describing a single one of the phosphate ligands found around Cu(II) in the pH 2 whole-cell sample.

In both the amine and carboxyl models, we fixed the numbers of oxide or amine groups in the first coordination sphere of the Cu at four, with up to two different Cu-N or Cu-O distances.

The distances describing the amine ligand structures found by refinements of the models are generally close to the distances in Cu phthalocyanine (11). The Cu-O distances describing the bidentate carboxyl ligand are close to the single Cu-O distance to the monodentate acetate ligands in $Cu(OAc)_2 \cdot H_2O$. The C-C distance in our carboxyl ligand, deduced from the difference between the Cu α-C and Cu β-C distances, is almost certainly too short at 1.0 Å if Cu α-C and β-C are colinear. The distance in the acetate groups of $Cu(OAc)_2 \cdot H_2O$ is 1.5 Å. One interpretation would be an angle of about 40° about the α-C, but we expect the hybridization on the oxygen atoms to force the complex to be flat. The β-C is included in the model because an interaction with the signal from more distant atoms alters the fit parameters describing nearer atoms. Rather, the distance found by our fit is probably incorrect because of the simplicity of our model. Because the two carbon atoms of the model ligand are colinear with the core Cu cation, there are two strong double-scattering paths and one strong triple-scattering path involving the β-C and the intermediate α-C. These paths have the same length as the single-scattering Cu β-C path, but have phases modified by the other scattering interactions and are all strong. Since our model included only single-scattering paths, it would be surprising

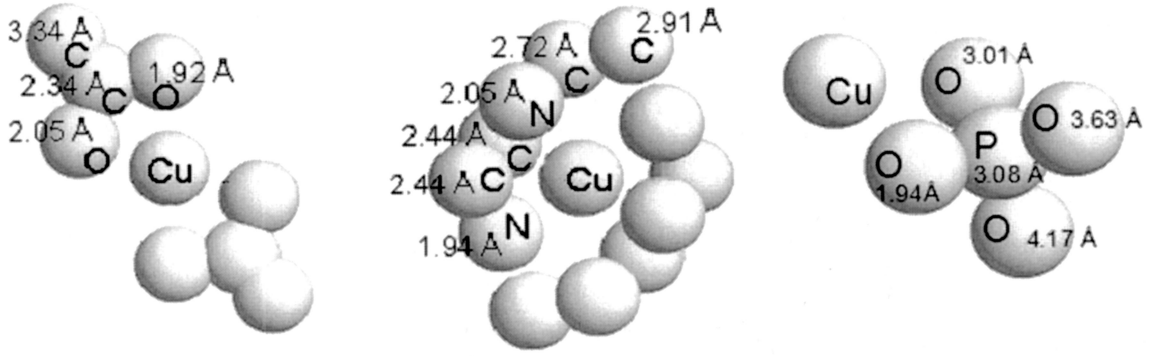

FIG. 6. Distances describing refined models for the carboxyl and amine structures, respectively, represent all the neighboring atoms to Cu located by analysis of EXAFS from carboxyl and amine chelating resins (left and middle). The refined distances are in good agreement with corresponding distances in $Cu(OAc)_2 \cdot H_2O$ and copper phthalocyanine. The structural parameters for a model comprising a monodentate phosphate anion are also shown (right).

if the β-C were described correctly. Debye-Waller factors were allowed to vary in the carboxyl model but were refined to small values. They were fixed at zero in the amine model. Since we fixed the coordination numbers at integer values and since coordination number and Debye-Waller factor values are usually correlated, the physical significance of fitted Debye-Waller factors would have been doubtful.

The single-scattering components of an EXAFS spectrum contain no bond angle information. It can be extracted from EXAFS by including multiple-scattering paths, which describe transverse distances between neighboring atoms (66). Multiple-scattering paths were not included in this analysis because their number grows rapidly with the complexity of the model. Also, they are more sensitive to structural disorder and complexity than single-scattering paths. Multiple-scattering paths that include transverse legs also increase the number of free variables used to fit data, while the associated contributions to the EXAFS are weak. Since the results here are based entirely on single-scattering paths, the atoms in Fig. 6 have not been shown to occupy the relative positions in the figures but may be located anywhere on the surfaces of spheres with the indicated radii. The relative positions shown in Fig. 6 incorporate reasonable assumptions about bond angles and connectivity.

DISCUSSION

Whole cells. Although the Cu described here was deposited onto lyophilized whole cells, we consider the possible relevance of our observations to the fate of Cu in living cells. As noted above, the Cu concentrations in our samples prepared in pH 5 aqueous 1,000-ppm Cu^{2+} were 26.8 mg g^{-1} for the whole-cell group and 90.4 mg g^{-1} for the cell wall group (37). These are 3 to 4 orders of magnitude above typical Cu concentrations found in live cyanobacteria. As reported by Jones et al. (30), the average concentration of Cu was 77 ppm (dry weight basis) among five cyanobacterial cultures grown in a nutrient medium containing 60 ppb of Cu^{2+}. Work by others (40) on *Anabaena* strain 7120 (ATCC27893) showed complete growth inhibition at approximately 126 ppm aqueous Cu^{2+}. The addition of 10^{-4} M Cu^{2+} to logarithmically growing and older cultures of *Anabaena* led to cell lysis.

Our data indicate that Cu in the whole-cell samples is coordinated exclusively by phosphate after Cu adsorption at pH 2, but carboxyl and amine ligands also coordinated Cu at pH 5. Kelly et al. observed the same types of environments for UO_2^{2+} cations adsorbed by *Bacillus subtilis* at pHs 1.67 to 4.80 (36). As a preferred binding site for metal ions (13, 18), phosphate is abundant in the lipopolysaccharide layer (LPS) and in the phospholipids that make up the outer membrane of gram-negative bacteria (8). In fact, due to its position on the outer leaflet of the outer membrane, the LPS is at the interface with extracellular metal ions. Beveridge, in his review of metal accumulation and mineralization by bacteria (9), asserts that the extent of participation of the peptidoglycan cell wall layer in mineral development is not clear, because it is positioned beneath the LPS. TEM indicated that mineralization takes place predominantly on the outer membrane and LPS (9). No mineralization was seen in the peptidoglycan (19).

Not all bacteria present phosphate sites in the LPS capable of binding metals. Work on four species of cyanobacteria found too little phosphorous in the core lipid A (0.03% in *A. variabilis*) to explain metals accumulation in this region by phosphate chelation (34). Yet in *Mycrocystis aeruginosa*, another cyanobacterium, the workers found significant amounts of phosphate in the LPS of two isolates (55). There are also numerous examples of metal ion binding to other bacterial LPS. For example, metal ions have been shown to bind to this layer in the gram-negative bacteria *Escherichia coli K-12* (10, 63). Other work has identified phosphate residues as the predominant ligands for metal cations in the *E. coli* K-12 outer membrane (18). Langley and Beveridge concluded from study of *Pseudomonas aeruginosa* that the phosphate metal binding sites are in the core-lipid A region of the LPS (39). Another study, of aquatic particles in a lake contaminated by zinc smelting operations, found zinc-phosphorous particles closely associated to "biological structures" (73). The authors inferred precipitation of phosphate compounds via an intra- or extra-cellular biological process. Another possible occurrence of phosphorous in metal binding involves phosphate pools and polyphosphate bodies in microbial cells. Polyphosphate bodies (PPBs) are phosphorous-rich granules present in cyanobacteria that may act as a sink for metals (29, 53). They have negatively charged surfaces that may serve as binding sites for metal ions (54). PPBs typically contain phosphorous, magnesium, sodium, potassium, and iron, and may serve a role in the detoxification of metals as well as the storage of phosphorous (67). *Anacystis nidulans* is one cyanobacterium that has been shown to accumulate Cu^{2+} principally in polyphosphate bodies (48). Other work supports the hypothesis that the ability to degrade polyphosphate to orthophosphate may serve as a metals detoxification mechanism in bacteria (1, 33, 74). In living cells, polyphosphate is degraded to orthophosphate by the enzyme polyphosphatase. Precipitated metal-phosphates are then transported out of the cells. This is corroborated by investigation of *Klebsiella* using Cd. Researchers saw a decrease in levels of polyphosphate followed by an increase in cell-associated orthophosphate (1). Work on Citrobacter illustrated the precipitation of metal-phosphates coinciding with the hydrolysis of organophosphates (25, 41, 42, 43).

The structural parameters determined by EXAFS fitting (supplemental material) indicate a relative decrease in phosphate coordination of Cu at pH 5 compared to pH 2. XANES analysis found substantial Cu(I) in that sample with amine and thiol ligands. Decreased phosphate coordination is also consistent with an increased role by other pH-sensitive ligands, such as carboxyl groups, present in the extracellular polysaccharides. The polysaccharides on the outer membrane of cyanobacteria are a possible binding site for metal ions due to the presence of uronic acids (64, 65). Experiments with the cyanobacterium *Phormidium valderianum* BDU 30501 suggested that carboxyl groups served as the main metal binding ligands (32). Experiments performed with *Synechococcus* strain 7942 whole cells also indicated that metals were binding to carboxyl groups (23, 24).

The presence of Cu(I) in whole cells is not unexpected. The presence inside cyanobacterial cells of metallothionein, a metal-binding protein, and other sulfhydryl and amine-containing proteins which bind Cu(I), was recently reviewed by Robinson (59).

Cell walls. Our results indicate that the Cu present in the cell wall peptidoglycan samples is coordinated by amine and bidentate carboxyl ligands. Researchers have previously identified the

peptidoglycan of the cell wall as a metal ion binding site (7, 26). Beveridge and Murray suggest that the glutamic acid present in the peptidoglycan of *B. subtilis* cell walls serves as the main ligand for metal ions (7). Work done on the peptidoglycan of *E. coli* K-12 also suggests the involvement of carboxyl groups in metal ion binding (26). Carboxyl groups are not the only possible ligands for Cu^{2+}; in fact, Cu^{2+} binds to amines before carboxyl groups (27).

A pH-dependent ion-exchange process is evident in binding by the cell wall samples. l-Meso-diaminopimelic acid is a bacterial and cyanobacterial cell wall constituent with an amine group available for metal ion binding. The peptidoglycan of cyanobacterial cell walls, of for example *Synechocystis* sp., contains the typical constituents of the A1 peptidoglycan type: a polymer of β-(1,4)-linkages of *N*-acetylglucosamine and *N*-acetylmuramic acid residues, cross-linked by L-alanine, D-glutamic acid, *meso*-diaminopimelic acid, and D-alanine (31). These results are consistent with a study on Cu ion binding by *Bacillus polymyxa* where it was found that Cu(II) was most likely binding to the oxygen atoms present on the carboxylic groups of the peptidoglycan and nitrogen atoms of structural proteins or amine sugars (50). Other groups that could participate in metal ion binding include hydroxyl, carboxyl, and amine.

Analysis of metals bound by these samples illustrates that these cells have several modes for sequestering Cu. A pH-dependent ion-exchange process is evident in binding by the cell wall samples. Binding of Cu(I) species by thiol or amine moieties is consistent with covalent bond formation in the whole-cells samples, and we believe there to be precipitation of Cu-phosphate species in whole-cell samples as well.

APPENDIX

TABLE A1. Structural parameters and standard deviations describing fits to EXAFS from Cu on carboxyl and amine chelating resins. The actual fits are plotted in Fig. 5A. Arrangements of atoms consistent with the structural parameters are shown in Fig. 6A.

	Carboxyl resin pH 5	Amine resin pH 5
Atom pair	Cu–O	Cu–N
Coord. No.	2	2
R/Å	1.92 ± 2e-3	1.94 ± 7e-3
σ^2/Å^2	1.1e-3 ± 6e-5	0
ΔE_o	−5.1 ± 6e-3	−7.2 ± 2e-2
Atom pair	Cu–O	Cu–N
Coord. No.	2	2
R/Å	2.05 ± 5e-4	2.05 ± 1e-2
σ^2/Å^2	1.1e-3 ± 6e-5	0
ΔE_o	5.1 ± 6e-3	−7.2
Atom pair	Cu–C	Cu–C
Coord. No.	2	2
R/Å	2.34 ± 4e-4	2.44 ± 5e-3
σ^2/Å^2	4.4e-3 ± 7e-5	0
ΔE_o	−5.9 ± 1e-2	−1.6 ± 2e-2
Atom pair	Cu–C	Cu–C
Coord. No.	2	2
R/Å	3.34 ± 1e-3	2.72 ± 5e-3
σ^2/Å^2	4.4e-3 ± 7e-5	0
ΔE_o	−5.9 ± 1e-2	−1.6
Atom pair		Cu–C
Coord. No.		2.1 ± 4e-1
R/Å		2.91 ± 1e-2
σ^2/Å^2		0
ΔE_o		−1.6

TABLE A2. Structural parameters describing phosphate coordination of Cu in whole-cell samples. Coordination numbers were all held equal to preserve the stoichiometry of the ligands. The fits used one ΔE_o value for the phosphorus and a second for all four oxygens. The MSRD parameter σ^2 was constrained to the range from 0 to 0.01 Å^2. Standard deviations are listed after parameter values. The actual fits are plotted in Fig. 5B. An arrangement of one phosphate group consistent with the pH 2 fit is shown in Fig. 6B.

	Whole cell pH 2	Whole cell pH 5
Atom pair	Cu–O	Cu–O
Coord. No.	3.9 ± 8e-3	2.7 ± 3e-3
R/Å	1.94 ± 3e-4	1.94 ± 1e-4
σ^2/Å^2	6.9e-3 ± 6e-5	4.1e-3 ± 2e-5
ΔE_o	−0.6 ± 1e-2	−6.1 ± 1e-2
Atom pair	Cu–O	Cu–O
Coord. No.	3.9	2.7
R/Å	3.01 ± 2e-3	3.15 ± 4e-3
σ^2/Å^2	0.01 ± 7e-4	1e-2 ± 4e-4
ΔE_o	−0.6	−6.1
Atom pair	Cu–P	Cu–P
Coord. No.	3.9	2.7
R/Å	3.08 ± 2e-3	3.10 ± 2e-3
σ^2/Å^2	8.9e-3 ± 3e-4	1e-2 ± 1e-4
ΔE_o	2.5 ± 7e-2	−6.2 ± 5e-2
Atom pair	Cu–O	Cu–O
Coord. No.	3.9	2.7
R/Å	3.63 ± 2e-3	3.66 ± 8e-4
σ^2/Å^2	0.01 ± 5e-4	1.0e-2 ± 2e-4
ΔE_o	−0.6	−6.1
Atom pair	Cu–O	Cu–O
Coord. No.	3.9	2.7
R/Å	4.17 ± 2e-3	4.23 ± 1e-3
σ^2/Å^2	8.0e-3 ± 4e-4	1.0e-2 ± 2e-4
ΔE_o	−0.6	6.1

ACKNOWLEDGMENTS

R. Webb acknowledges support from NIH NCRR Research Centers in Minority Institutions grant G12RR08124 and NIH Score program grant S06GM8012-28. We acknowledge financial support from the University of Texas at El Paso Center for Environmental Resource Management through funding from the Office of Exploratory Research of the EPA (cooperative agreement CR-819849-01-4). J. L. Gardea-Torresdey acknowledges funding from the National Institutes of Health Score program (grant S06GM8012-30).

Portions of this research were carried out at the Stanford Synchrotron Radiation Laboratory, a national user facility operated by Stanford University on behalf of the U.S. Department of Energy, Office of Basic Energy Sciences. The SSRL Structural Molecular Biology Program is supported by the Department of Energy, Office of Biological and Environmental Research, and by the National Institutes of Health, National Center for Research Resources, Biomedical Technology Program. In addition, we acknowledge the SSRL/DOE-funded gateway program.

REFERENCES

1. **Aiking, H., A. Stijnman, C. van Garderen, H. van Heerikhuizena, and J. van't Riet.** 1984. Inorganic phosphate accumulation and cadmium detoxification in *Klebsiella aerogenes* NCTC 418 growing in continuous culture. Appl. Environ. Microbiol. **47:**374–377.
2. **Allen, M. J.** 1968. Simple conditions for growth of unicellular blue-green algae on plates. Phycology **4:**1–4.
3. **Ankudinov, A. L., B. Ravel, J. J. Rehr, and S. D. Conradson.** 1998. Real-space multiple-scattering calculation and interpretation of X-ray-absorption near-edge structure. Phys. Rev. B **58:**7565–7576.
4. **Ankudinov, A. L., and J. J. Rehr.** 2000. Theory of solid-state contributions to the X-ray elastic scattering amplitude. Phys. Rev. B **62:**2437–2445.
5. **Bacon, G. E., and N. A. Curry.** 1962. The water molecules in $CuSO_4 \cdot 5H_2O$. Proc. R. Soc. Lond. A **266:**95–108.
6. **Barkay, T., and J. Schaefer.** 2001. Metal and radionuclide bioremediation: issues, considerations and potentials. Curr. Opin. Microbiol. **4:**318–323.
7. **Beveridge, T. J., and G. E. Murray.** 1980. Sites of metal deposition in the cell wall of *Bacillus subtilis.* J. Bacteriol. **141:**876–887.

8. **Beveridge, T. J., and W. S. Fyfe.** 1985. Metal fixation by bacterial cell walls. Can. J. Earth Sci. **22:**1893–1898.
9. **Beveridge, T. J.** 1989. Role of cellular design in bacterial metal accumulation and mineralization. Annu. Rev. Microbiol. **43:**147–171.
10. **Beveridge, T. J., and S. F. Koval.** 1981. Binding of metals to cell envelopes of *Escherichia coli* K-12. Appl. Environ. Microbiol. **42:**325–335.
11. **Brown, C. J.** 1968. Crystal structure of β-copper phthalocyanine. J. Chem. Soc. A **10:**2488–2493.
12. **Cavet, J. S., G. P. M. Borrelly, and N. J. Robinson.** 2003. Zn, Cu and Co in cyanobacteria: selective control of metal availability. FEMS Microbiol. Rev. **27:**165–181.
13. **Couglin, R. T., S. Tonsager, and E. McGroar.** 1983. Quantitation of metal cations bound to membranes and extracted lipopolysaccharide of *Escherichia coli.* J. Biochem. **22:**2002–2007.
14. **Daughney, C. J., J. B. Fein, and N. Yee.** 1998. A comparison of the thermodynamics of metal adsorption onto two common bacteria. Chem. Geol. **144:**161–176.
15. **El Meskini, R., V. C. Culotta, R. E. Mains, and B. A. Eipper.** 2003. Supplying copper to the cuproenzyme peptidylglycine α-amidating monooxygenase. J. Biol. Chem. **278:**12278–12284.
16. **Fein, J. B., C. J. Daughney, N. Yee, and T. A. Davis.** 1997. A chemical equilibrium model for metal adsorption onto bacterial surfaces. Geochim. Cosmochim. Acta **61:**3319–3328.
17. **Fenton, D. E.** 1995. *In* Biocoordination chemistry. Oxford University Press, Inc., New York, N.Y.
18. **Ferris, F. G., and T. J. Beveridge.** 1986. Site specificity of metallic ion binding in Escherichia coli K-12 lipopolysaccharide. Can. J. Microbiol. **32:**52–55.
19. **Ferris, F. G., T. J. Beveridge, and W. S. Fyfe.** 1986. Iron-silica crystallite nucleation by bacteria in a geothermal sediment. Nature **320:**609–611.
20. **Fowle, D. A., J. B. Fein, and A. M. Martin.** 2000. Experimental study of uranyl adsorption onto *Bacillus subtilis.* Environ. Sci. Technol. **34:**3737–3741.
21. **Gardea-Torresdey, J. L., I. Cano-Aguilera, R. Webb, K. J. Tiemann, and F. Gutierrez-Corona.** 1996. Copper adsorption by inactivated cells of *Mucor rouxii*: effect of esterification of carboxyl groups. J. Hazardous Mat. **48:**171–180.
22. **Gardea-Torresdey, J. L., S. Arteaga, K. J. Tiemann, R. Chianelli, N. Pingitore, and W. Mackay.** 2001. Absorption of copper(II) by creosote bush (Larrea tridentata): use of atomic and X-ray absorption spectroscopy. Environ. Tox. Chem. **20:**2572–2579.
23. **Gardea-Torresdey, J. L., J. L. Arenas, R. Webb, N. M. C. Francisco, and K. J. Tiemann.** 1998. Ability of immobilized cyanobacteria to remove metal ions from solution and demonstration of the presence of metallothionein genes in various strains. J. Hazard. Subst. Res. **1:**1–18.
24. **Gardea-Torresdey, J. L., J. L. Arenas, R. Webb, and K. J. Tiemann.** 1998. Effects of carboxyl group esterification on metal binding ability of *Synechococcus* sp. PCC 7942 (*Cyanobacteria*), p. 105–109. *In* Proceedings of the Joint Conference on the Environment. Kansas State University, Manhattan.
25. **Hambling, S. G., L. E. Macaskie, and A. C. R. Dean.** 1987. Phosphatase synthesis in a *Citrobacter* sp. growing in continuous culture. J. Gen. Microbiol. **133:**2743–2749.
26. **Hoyle, B. D., and T. J. Beveridge.** 1984. Metal binding by the peptidoglycan sacculus of *Escherichia coli* K-12. Can. J. Microbiol. **30:**204–211.
27. **Hughes, M. N.** 1974. The inorganic chemistry of biological processes, p. 63–104. John Wiley and Sons, New York, N.Y.
28. **Iwamoto, T., and M. Nasu.** 2001. Current bioremediation practice and perspective. Biosci. Bioeng. **92:**1–8.
29. **Jensen, T. E., M. Baxter, J. W. Rachlin, and V. Jani.** 1982. Uptake of heavy metals by Plectonema boryanum (Cyanophyceae) into cellular components, especially polyphosphate bodies: an X-ray energy dispersive study. Environ. Pollut. **27:**119–127.
30. **Jones, G. E., L. Murray, and N. G. Carr.** 1977. *In* W. E. Krumbein (ed.), Proceedings of the 3rd International Symposium on Environment, Biogeochemistry, and Geomicrobiology, p. 967–973. Ann Arbor Science, Ann Arbor, Mich.
31. **Jürgens, U. J., G. Drews, and J. Weckesser.** 1983. Primary structure of the peptidoglycan from the unicellular cyanobacterium *Synechocystis* sp. strain PCC 6714. J. Bacteriol. **154:**471–478.
32. **Karna, R. R., L. Uma, G. Subramanian, and P. M. Mohan.** 1999. Biosorption of toxic metal ions by alkali-extracted biomass of a marine cyanobacterium, Phormidium valderianum BDU 30501. World J. Microbiol. Biotechnol. **15:**729–732.
33. **Keasling, J. D.** 1997. Regulation of intracellular toxic metals and other cations by hydrolysis of polyphosphate. Ann. N. Y. Acad. Sci. **829:**242–249.
34. **Keleti, G., and J. L. Sykora.** 1982. Production and properties of cyanobacterial endotoxins. Appl. Environ. Microbiol. **43:**104–109.
35. **Kelly, S. D., M. I. Boyanov, B. A. Bunker, J. B. Fein, D. A. Fowle, N. Yee, and K. M. J. Kemner.** 2001. XAFS determination of the bacterial cell wall functional groups responsible for complexation of Cd and U as a function of pH. Synchrotron Rad. **8:**946–948.
36. **Kelly, S. D., K. M. Kemner, J. B. Fein, D. A. Fowle, M. I. Boyanov, B. A. Bunker, and N. Yee.** 2002. X-ray absorption fine structure determination of pH-dependent U-bacterial cell wall interactions. Geochim. Cosmochim. Acta **66:**3855–3871.
37. **Kretschmer, X. C., J. Gardea-Torresdey, R. R. Chianelli, and R. Webb.** 2002. Determination of copper binding in *Anabaena flos-aquae* purified cell walls and whole cells by X-ray absorption spectroscopy. Microchem. J. **71:**295–304.
38. **Kunzl, V.** 1932. Linear dependence of energy levels on the valency of elements. Colloq. Czech Chem. Comm. **4:**213–224.
39. **Langley, S., and T. J. Beveridge.** 1999. Effect of O-side-chain-lipopolysaccharide chemistry on metal binding. Appl. Environ. Microbiol. **65:**489–498.
40. **Laube, V. M., C. N. McKenzie, and D. J. Kushner.** 1980. Strategies of response to copper, cadmium, and lead by a blue-green and a green alga. Can. J. Microbiol. **26:**1300–1311.
41. **Macaskie, L. E., and A. C. R. Dean.** 1984. Cadmium accumulation by a Citrobacter sp. J. Gen. Microbiol. **130:**53–62.
42. **Macaskie, L. E., A. C. R. Dean, A. K. Cheetham, R. J. B. Jakeman, and A. J. Skarnulis.** 1987. Cadmium accumulation by a *Citrobacter* sp.: the chemical nature of the accumulated metal precipitate and its location on the bacterial cells. J. Gen. Microbiol. **133:**539–544.
43. **Macaskie, L. E., R. M. Empson, A. K. Cheetham, C. P. Grey, and A. J. Skarnulis.** 1992. Uranium bioaccumulation by a *Citrobacter* sp. as a result of enzymatically mediated growth of polycrystalline HUO2PO4. Science **257:**782–784.
44. **Malinowski, E. R., and D. G. Howery.** 1981. Factor analysis in chemistry. John Wiley & Sons, New York, N.Y.
45. **McMaster, H., N. K. Del Grande, J. H. Mallet, and J. H. Hubbell.** 1978. Compilation of X-ray cross sections. Report UCRL-50174, sec. II, rev. 1. Lawrence Radiation Laboratory, UC Livermore, Livermore, Calif.
46. **Mehrabi, S., U. M. Ekanemasang, F. O. Aikhionbare, K. S. Kimbro, and J. Bender.** 2001. Identification and characterization of Rhodopseudomonas sp., a purple, non-sulfur bacterium from microbial mats. Biomol. Eng. **18:**49–56.
47. **Meitzner, G., and E. S. Huang.** 1992. Analysis of mixtures of compounds of copper using K-edge X-ray absorption spectroscopy. Fresnius J. Anal. Chem. **342:**61–64.
48. **Pandey, U., and A. Mishra.** 1998. Cu^{2+} and Cd^{2+} uptake and their localization in cyanobacterium *Anacystis nidulans.* J. Ecotox. Environ. Monitoring **8:**179–182.
49. **Parsons, J. G., M. Hajazi, K. J. Tiemann, J. Hennings, and J. L. Gardea-Torresdey.** 2002. An XAS study of the binding of copper(II), zinc(II), chromium(III) and chromium(VI) to hops biomass. Microchem. J. **71:**211–219.
50. **Philip, L., and C. Venkobachar.** 2001. An insight into the mechanism of biosorption of copper by Bacillus polymyxa. Int. J. Environ. Pollut. **15:**448–460.
51. **Polette, L. A., J. L. Gardea-Torresdey, R. R. Chianelli, G. N. George, I. Pickering, and J. Arenas.** 2000. XAS and microscopy studies of the uptake and bio-transformation of copper in *Larrea tridentata* (creosote bush). Microchem. J. **65:**227–236.
52. **Prins, R., and D. C. Koningsberger.** 1988. Theory of EXAFS, p. 3−51. *In* D. C. Koningsberger and R. Prins (ed.), X-ray absorption: principles, applications, techniques of EXAFS, SEXAFS, and XANES. Wiley Interscience, New York, N.Y.
53. **Rachlin, J. W., T. E. Jensen, and B. Warkentine.** 1985. Morphometric analysis of the response of Anabaena flos-aquae and Anabaena variabilis (Cyanophyceae) to selected concentrations of zinc. Arch. Environ. Contamin. Toxicol. **14:**395–402.
54. **Rangsayatorn, N., E. S. Upatham, M. Kruatrachue, P. Pokethitiyook, and G. R. Lanza.** 2002. Phytoremediation potential of *Spirulina* (*Arthrospira*) *platensis*: biosorption and toxicity studies of cadmium. Environ. Pollut. **119:**45–53.
55. **Raziuddin, S., H. W. Siegelman, and T. G. Tornabene.** 1983. Lipopolysaccharides of the cyanobacterium Microcystis aeruginosa. Eur. J. Biochem. **137:**333–336.
56. **Ressler, T., J. Wong, J. Roos, and I. L. Smith.** 2000. Quantitative speciation of Mn-bearing particulates emitted from autos burning (methylcyclopentadienyl) manganese tricarbonyl-added gasolines using XANES spectroscopy. Environ. Sci. Technol. **34:**950–958.
57. **Ressler, T.** 1998. WinXas: a program for X-ray absorption spectroscopy data analysis under MS-Windows. J. Synchrotron Rad. **5:**118–122.
58. **Ressler, T.** 1997. WinXas: a new software package not only for the analysis of energy dispersive XAS data. J. Physique IV **7:**269–270.
59. **Robinson, N. J., S. K. Whitehall, and J. S. Cavet.** 2001. Microbial metallothioneins. Adv. Microbiol. Physiol. **44:**183–213.
60. **Sarret, G., A. Manceau, L. Spadini, J.-C. Roux, J.-L. Hazemann, Y. Soldo, L. Eybert-Bérard, and J. Menthonnex.** 1998. Structural determination of Zn and Pb binding sites in Penicillium chrysogenum cell walls by EXAFS spectroscopy. J. Environ. Sci. Technol. **32:**1648–1655.
61. **Shoemaker, G. L., J. B. Anderson, and E. Kostiner.** 1977. Copper(II) phosphate. Acta Crystallogr. B **33:**2969–2972.
62. **Solioz, M., and J. V. Stoyanov.** 2003. Copper homeostasis in *Enterococcus hirae.* FEMS Microbiol. Rev. **27:**183–195.
63. **Strain, S. M., S. W. Fesik, and I. M. Armitage.** 1983. Structure and metal-binding properties of lipopolysaccharides from heptoseless mutants of Esch-

erichia coli studied by ^{13}C and ^{31}P nuclear magnetic resonance. J. Biol. Chem. **258:**13466–13477.
64. **Subramanian, G., and L. Uma.** 1996. Cyanobacteria in pollution control. J. Sci. Indust. Res. **55:**685–692.
65. **Sutherland, R. J., and M. I. Tait.** 1992. *In* J. Lederberg (ed.), Encyclopedia of microbiology, vol. 1 Biopolymers. p. 339–349. Academic Press, San Diego, Calif.
66. **Teo, B. K.** 1981. Novel method for angle determinations by EXAFS via a new multiple-scattering formalism. J. Am. Chem. Soc. **103:**3990−4001.
67. **Thomas, E. J.** 1993. Cyanobacterial ultrastructure, p. 8–51. *In* B. Tarmar (ed.), Ultrastructure of microalgae. CRC Press, Boca Raton, Fla.
68. **Tiemann, K. J., A. E. Rascon, G. Gamez, J. G. Parsons, T. Baig, I. Cano-Aguilera, and J. L. Gardea-Torresdey.** 2002. Heavy metal binding by inactivated tissues of Solanum elaeagnifolium: chemical and subsequent XAS studies. Microchem. J. **71:**133–141.
69. **Tottey, S., S. A. M. Rondet, G. P. M. Borrelly, P. J. Robinson, P. R. Rich, and N. J. Robinson.** 2002. A copper metallochaperone for photosynthesis and respiration reveals metal-specific targets, interactions with an importer, and alternative sites for copper acquisition. J. Biol. Chem. **277:**5490–5497.
70. **Van Niekerk, J. N., and F. R. L. Schoening.** 1953. X-ray evidence for metal-to-metal bonds in cupric and chromous acetate. Nature **171:**36–37.
71. **Weast, R. C. (ed.).** 1988. CRC handbook of chemistry and physics. CRC Press, Inc., Boca Raton, Fla.
72. **Webb, S. M., J.-F. Gaillard, B. E. Jackson, and D. A. Stahl.** 2001. An EXAFS study of zinc coordination in microbial cells. J. Synchrotron Rad. **8:**943–945.
73. **Webb, S. M., G. G. Leppard, and J. F. Gaillard.** 2000. Zinc speciation in a contaminated aquatic environment: characterization of environmental particles by analytical electron microscopy. Environ. Sci. Technol. **34:**1926–1933.
74. **Zhang, W., and V. Majidi.** 1994. Monitoring the cellular response of *Stichococcus bacillaris* to exposure of several different metals using in vivo 31P NMR and other spectroscopic techniques. Environ. Sci. Technol. **28:**1577–1581.